Biosensors and Bioelectronics 126 (2019) 222–229

Contents lists available at ScienceDirect

Biosensors and Bioelectronics

journal homepage: www.elsevier.com/locate/bios

CuS as co-reaction accelerator in PTCA-$K_2S_2O_8$ system for enhancing electrochemiluminescence behavior of PTCA and its application in detection of amyloid-β protein

Xianzhen Song, Xiaojian Li, Dong Wei, Rui Feng, Tao Yan, Yaoguang Wang, Xiang Ren, Bin Du, Hongmin Ma*, Qin Wei

Key Laboratory of Interfacial Reaction & Sensing Analysis in Universities of Shandong, School of Chemistry and Chemical Engineering, University of Jinan, Jinan 250022, China

ARTICLE INFO

Keywords:
PTCA
CuS
Co-reaction accelerator
Amyloid-β protein

ABSTRACT

In this work, 3,4,9,10-perylenetetracar-boxylic acid (PTCA) as luminophor was grafted on the surface of graphene oxide (PTCA-GO) directly. GO exhibited large specific surface area and excellent electrical conductivity which can immobilize large amounts of PTCA to improve the electrochemiluminescence (ECL) efficiency. Moreover, gold nanoparticles (Au NPs) were anchored on the surface of PTCA-GO to immobilize primary antibodies (Ab_1) via Au-NH_2 bond and enhance the electron transport of PTCA-GO. CuS was used as a novel co-reaction accelerator in PTCA-$K_2S_2O_8$ system to label secondary antibodies (Ab_2), which can react with the coreactant ($K_2S_2O_8$) to produce more $SO_4^{\bullet-}$. SiO_2 nanospheres with large specific surface area were used to load a mass of CuS and Au NPs, which can directly combine with Ab_2 and accelerate the ECL emission remarkably. Therefore, a novel sandwich-type ECL immunosensor was fabricated successfully for amyloid-β protein (Aβ) detection. Under the optimal condition, a wide detection range from 50 fg/mL to 25 ng/mL and a low detection limit of 18 fg/mL (S/N = 3) were obtained. Featuring favorable specificity, stability and reproducibility, the strategy can be a powerful analytical tool in sensitive trace detection of biomolecules in clinical analysis.

1. Introduction

Alzheimer's disease (AD) is a progressive neuromuscular atrophy, which is initially characterized by learning and memory impairment that will eventually lead to loss of cognitive ability (Selkoe and Schenk, 2003). Furthermore, it is the most common cause of dementia among older adults. The genetic studies have shown that amyloid-β proteins (Aβ) play a key role in the development of AD (Nhan et al., 2015; Selkoe, 2001). Therefore, many methods have been developed to quantify Aβ. For instance, chemiluminescence (Nishikimi et al., 2013), radioimmunoassay (Cowie et al., 2003), surface plasmon resonance immunoassays (Jang et al., 2014) and so on. At present, the application of electrochemiluminescence (ECL) technology in the detection of Aβ has attracted more attention because of it's simple and sensitive. In this work, a novel sandwich-type ECL immunosensor was fabricated for highly sensitive detection of Aβ based on PTCA-Au@GO and CuS-Au@SiO_2 nanomaterials.

3,4,9,10-perylenetetracar-boxylic acid (PTCA) is the hydrolysis product of perylene-3,4,9,10-tetracarboxylic dianhydride (PTCDA). It is a 5-ring polycyclic aromatic hydrocarbon that modified with abundant carboxyl groups, and the perylene derivates with branched chains indicate that it has many advantages. For instance, the unique structure of PTCA can not only reduce biological toxicit, but also increase its hydrophobicity (Jana et al., 2012, 2014). In this work, PTCA was used as ECL luminophore to react with coreactant ($K_2S_2O_8$) for constructing the solid-state ECL sensor platform in Aβ detection. GO exhibited excellent electrical conductivity and large specific surface area which was used to load large amounts of PTCA. In addition, Au NPs were anchored on the surface of PTCA@GO can not only combine with Ab_1, but also enhance the electrical transfer.

As a well-known p-type semiconductor material, copper sulfide (CuS) has applications in many different fields (Tan and Wang, 2010), such as catalysis (Dubale et al., 2016; Hong et al., 2015), biosensors (Goel et al., 2013), superconductor (Mazin, 2012), cancer and antibacterial (Shuang et al., 2015), microwave absorption (Zhou et al., 2015), energy conversion and storage (Feng et al., 2015; Lee et al., 2007) and so on. As we all know, many copper compounds exhibit quite high catalytic performance (Liu et al., 2016). For instance, some copper

* Corresponding author.
E-mail address: mahongmin2002@126.com (H. Ma).

https://doi.org/10.1016/j.bios.2018.10.068
Received 6 August 2018; Received in revised form 15 October 2018; Accepted 30 October 2018
Available online 02 November 2018
0956-5663/

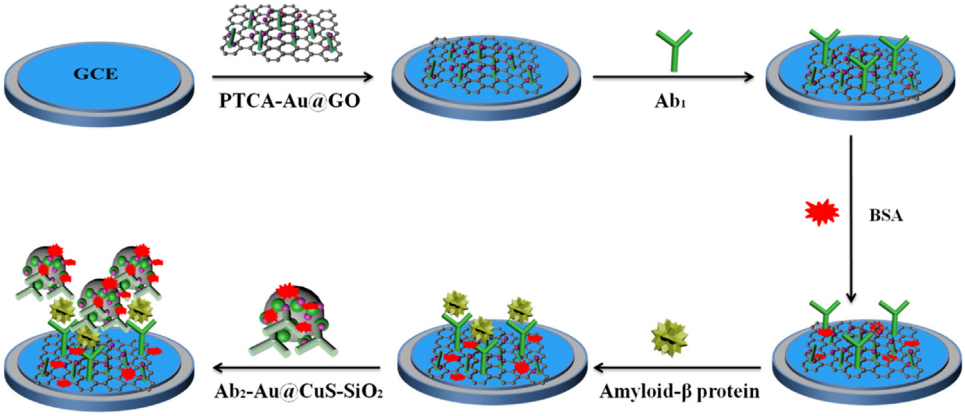

Fig. 1. Schematic representation of the fabrication of immunosensor.

compounds act as fenton-like reagents which can catalyze H_2O_2 producing $OH^{\bullet}$ (Dutta et al., 2013). In this work, CuS acted as co-reaction accelerator to catalyze $K_2S_2O_8$ producing more $SO_4^{\bullet-}$, further enhancing the ECL signal of PTCA. SiO_2 nanospheres were used to load a mass of CuS and Au NPs as a result of its large specific surface area, which could combine with Ab_2 and improve the ECL efficiency.

Herein, a sensitive and stable sandwich ECL immunosensor was prepared for Aβ detection. As shown in Fig. 1, the detailed fabrication process of the immunosensor was observed. First, PTCA-Au@GO solution was dropped on the surface of glassy carbon electrode (GCE). Subsequently, primary antibody (Ab_1) was dropped on the modified surface of GCE. Next, bovine serum albumin (BSA) was dispersed on the modified surface of GCE to block nonspecific binding. Then the Aβ with different concentrations were dropped on the modified surface of GCE. Finally, the prepared Ab_2-Au@CuS-SiO_2 solution was incubated with the modified GCE.

2. Experimental section

2.1. Materials

Amyloid-β protein (Aβ), amyloid-β protein primary antibody (Ab_1) and secondary antibody (Ab_2) were obtained from Nanjing Kingsrui Technology CO. LTD. BSA (96–99%) was purchased from Aladdin Industrial Corporation. Ethanol, methylbenzene, sodium citrate, sodium hydroxide (NaOH), sodium borohydride ($NaBH_4$), aminopropyltriethoxysilane (APTES), potassium persulfate ($K_2S_2O_8$), polyvinylpyrrolidone (PVP) and $HAuCl_4{\cdot}6H_2O$ were obtained from Sinopharm Chemical. PTCDA was purchased from TOKYO Chemical Industry CO. LTD. All the chemicals that used without further purification were of analytical reagent grade. Phosphate buffered saline (PBS) was prepared by mixing 1/15 Na_2HPO_4 and 1/15 KH_2PO_4. The electrolyte for electrochemical impedance spectroscopy (EIS) was prepared by 0.1 M KNO_3 and 2.5 mM $[Fe(CN)_6]^{3-/4-}$ solution. Chitosan was dissolved in 1% acetic acid and ultrapure water (18.25 MΩ cm, 24 °C) was used for all the experiments.

2.2. Apparatus

X-ray powder diffraction (XRD) was performed with a D8 advance X-ray diffractometer (Bruker AXS, Germany). UV–vis measurements were carried out on a Lambda 35 UV–vis spectrometer (PerkinElmer, United States). X-ray photoelectron spectroscopy (XPS) spectra was recorded with an Escalab MK II (VG Company, UK). Scanning electron microscope (SEM) and transmission electron microscopy (TEM) images were gained by JEOL JSM-6700F microscope (Japan). The ECL measurements were carried out by using MPI-F flowinjection chemiluminescence detector (Xi'an remax Electronic Science Tech. Co. Ltd., China) and electrochemical measurements were performed with CHI760D electrochemical workstation (Chenhua Instrument Shanghai Co. Ltd., China). A three-electrode system consisted of a platinum wire acted as auxiliary electrode, an Ag/AgCl electrode acted as reference electrode and a glassy carbon electrode (GCE) (4 mm in diameter) acted as working electrode.

2.3. Preparation of PTCA and PTCA-Au@GO composites

PTCA nanomaterials were synthesized according to the previous paper (Zhuo et al., 2014). First, 10 mg PTCDA was dissloved in 10 mL of freshly prepared NaOH solution (1 M), then heated the solution until PTCDA dissolved completely and the color of the solution changed into yellow-green. Subsequently, HCl (1 M) was added into the above solution until the color of the mixture turn to red completely. Next, the resulted product was collected by centrifuging and washing, and the precipitate was washed with anhydrous ethanol and ultrapure water alternately until the pH was 7.4. Finally, the product was dried in vacuum at room temperature.

Graphene oxide (GO) was prepared by a modified Hummers' method from graphite powder (Marcano et al., 2010), and the detailed experiment process was showed in Supplementary material. PTCA@GO nanomaterials were synthesized as follows: 0.05 g GO was dissloved in ultrapure water, then the solution was ultrasounded for 1 h to make GO dissolve thoroughly. Subsequently, PTCA was added into the above solution and the mixture was ultrasounded for 2 h until GO and PTCA mixed well, then the above mixture was stirred for 12 h. PTCA@GO nanomaterials were finally obtained by centrifuging, washing and drying. For the synthesis of PTCA-Au@GO composites, 50 mg PTCA@GO nanomaterials were first dissolved in ultrapure water with ultrasonication for 2 h. Then 1 mL of $HAuCl_4$ (1%) and 10 mg PVP were added into the above solution with stirring for 12 h. Next, 4 mL of 50 mM sodium citrate and a little bit of $NaBH_4$ were added into the mixture with stirring for 12 h to reduce redundant $HAuCl_4$, then the PTCA-Au@GO suspension was washed with ultrapure water and anhydrous ethanol to remove unbonded Au NPs. Finally, the resulted product was dispersed in 0.5% chitosan for further use.

2.4. Preparation of Ab_2-Au@CuS-SiO_2 composites

SiO_2 was prepared as mentioned in the previous paper (Jia et al., 2015), and the detailed experimental process was showed in Supplementary material. CuS was synthesized based on the previous paper (Qiao et al., 2013), and the detailed experimental procedure was also showed in Supplementary material.

For the synthesis of Ab_2-Au@CuS-SiO_2 composites, CuS@SiO_2 nanomaterials were first synthesized. The prepared process of CuS@SiO_2 nanomaterials were as follows: 1 g SiO_2 was dissolved in 200 mL of

toluene, then 2 mL of APTES was added into the solution with ultrasonication for 0.5 h. Subsequently, the mixture was transferred into the Teflon-line stainless-steel autoclave (100 mL cubage) and maintained at 90 °C for 24 h. The aminated silica was obtained by centrifuging, washing and vacuum drying. Next, 10 mg prepared CuS was dissolved in ultrapure water, then 10 mg aminated silica was added into the mixture with stirring for 1.5 h. CuS@SiO_2 nanomaterials were finally obtained and the resulted product was dissolved in ultrapure water for further use. For the synthesis of Ab_2-Au@CuS-SiO_2 composites, 1 mL of $HAuCl_4$ (1%) and 10 mg PVP were first added into the above prepared solution with stirring for 12 h. Subsequently, 4 mL of sodium citrate solution (50 mM) and a little bit of $NaBH_4$ were added into the mixture with stirring for 12 h, then the CuS-Au@SiO_2 suspension was washed with ultrapure water and anhydrous ethanol. Next, the resulted product was dispersed in PBS (pH = 7.4) and mixed with Ab_2, then BSA was added into the above solution to block nonspecific binding. Finally, the mixture was stored at 4 °C for further use.

2.5. Preparation of the ECL immunosensor

Fig. 1 revealed the fabrication procedure of the ECL immunosensor. First, GCE was polished to a mirror-like surface with alumina powder (1.0, 0.3 and 0.05 μm), then it was cleaned with ultrapure water and dried in air. Subsequently, 8 μL of 1 mg/mL PTCA-Au@GO mixture was dropped on the surface of GCE. Then 5 μL of 1 mg/mL Ab_1 was dropped on the modified GCE surface and incubation at 4 °C for 2 h. What's more, for each modification step, the electrode was washed with ultrapure water to eliminate the nonspecific binding during the fabrication of the immunosensor. Next, 3 μL of 1 wt% BSA was dispersed on the modified GCE surface for 1.5 h to block nonspecific binding. Then 6 μL of prepared Aβ solution with different concentrations were dropped on the modified surface of GCE and incubated it at 4 °C for 3 h. Finally, the prepared Ab_2-Au@CuS-SiO_2 solution (7 μL of 2 mg/mL) was dropped on the modified GCE surface and maintained at 4 °C for 1.5 h.

2.6. ECL detection of Aβ

10 mL of PBS (pH = 8.5) containing 50 mM $K_2S_2O_8$ and 0.1 M KCl was added into the ECL cell. The scanning potential was set from −1.6–0 V, and the photomultiplier tube (PMT) was set at 600 V with scan rate of 0.1 V/s. Finally, the modified electrode was placed in the ECL cell, and the ECL signal was measured by a three-electrode system.

3. Result and discussion

3.1. Characterization of different nanomaterials

The morphologies of PTCA, PTCA@GO, PTCA-Au@GO, CuS, CuS@SiO_2 and CuS-Au@SiO_2 nanomaterials were investigated by SEM and TEM. As shown in Fig. 2A, PTCA nanomaterials exhibited short rod-like structure. According to Fig. 2B and C, PTCA nanomaterials were homogeneously distributed throughout the surface of GO, and Au NPs were anchored on the surface of PTCA@GO. As shown in Fig. 2E, CuS nanomaterials displayed sphere-like shape, and its diameter was about 20 nm. According to Fig. 2F and G, CuS nanospheres were homogeneously distributed on the surface of SiO_2, and Au NPs were anchored on the surface of CuS@SiO_2. As shown in Fig. S1, GO exhibited flake-like shape. SiO_2 nanomaterials exhibited sphere-like shape, which diameter was about 450 nm.

According to Fig. 2D, the XRD pattern of PTCA (a) showed four peaks which were at 12.2° (111), 16.7° (010), 22.7° (102) and 27.3° (201). The XRD pattern of GO (b) showed a characteristic peak which were at 14.9° (120). The above results were in good agreement with the previous paper (Li et al., 2009; Wang et al., 2016), which indicated that PTCA and GO nanomaterials were synthesized successfully. The characteristic peaks of GO and PTCA were showed in the XRD pattern of PTCA-Au@GO (c). Furthermore, the peak of PTCA-Au@GO at 38.3° was in good agreement with the characteristic peak of Au NPs (Karpenko et al., 2007). Therefore, it was inferred that PTCA-Au@GO nanomaterials were synthesized successfully. As shown in Fig. S2A, the XRD pattern of CuS exhibited eight diffraction peaks which were indexed at 27.7° (101), 29.3° (102), 31.8° (103), 32.9° (006), 38.8° (105), 47.9° (110), 52.7° (108) and 59.3° (116) (JCPDS No. 06-0464). As shown in Fig. S2B, the XRD pattern of SiO_2 exhibited four diffraction peaks which were indexed at 22.0° (101), 36.2° (200), 42.8° (211) and 45.0° (202) (JCPDS No. 06-0464). The results indicated that CuS and SiO_2 nanomaterials were synthesized successfully. As shown in Fig. 2H, the diffraction peaks of CuS-Au@SiO_2 were in good agreement with the peaks of CuS and SiO_2. Moreover, the diffraction peak of CuS-Au@SiO_2 at 38.3° (111) was in good agreement with the characteristic peak of Au NPs (Karpenko et al., 2007). Therefore, it was inferred that CuS-Au@SiO_2 nanomaterials were synthesized successfully.

XPS was used to further investigate the surface electronic state and elemental composition of the composite. According to Fig. S3A, the peaks of O 1s, C 1s and Au 4f were clearly observed in the XPS full survey spectrum of PTCA-Au@GO. As shown in Fig. S3B, the binding energies at 284.8, 286.2, 288.7 and 289.6 eV were due to C-C (284.8 eV), C-O (286.2 eV), C=O (288.7 eV), O-C=O (289.6 eV) groups (Li et al., 2018; Zhao et al., 2017), respectively. As shown in Fig. S3C, the O 1 s spectrum was fitted with three peaks at 531.7, 532.6 and 533.3 eV, which could be attributed to O-H (531.7 eV), O-C=O (532.6 eV) and C-O (533.3 eV) groups (Cai et al., 2016; Ma et al., 2017b), respectively. Therefore, it was inferred that the above peaks could be attributed to the hydroxy, carboxyl and epoxy in PTCA and GO. According to Fig. S4A, the peaks of Cu 2p, S 2p, O 1s, C 1s, Si 2p and Au 4f were clearly observed in the XPS full survey spectrum of CuS-Au@SiO_2. As shown in Fig. S4B, the binding energies at 103.8 eV correspond to Si 2p (Chung et al., 2011). As shown in Fig. S4C, the Cu 2p1/2 peak was fitted with two peaks at 952.5 and 954.5 eV, and the Cu 2p3/2 peak was fitted with three peaks at 934.7, 933.7 and 932.6 eV. The peak-to-peak separations between the Cu 2p1/2 (952.5 eV) and Cu 2p3/2 (932.6 eV) were about 20.0 eV, which indicated the typical values for Cu^{2+} in CuS materials (Nie et al., 2013). The binding energies of 954.5 and 933.7 eV could be CuS-$CuSO_4$ (Thuy et al., 2014), and the peak at 934.7 eV could be CuO (Tian et al., 2014). As shown in Fig. S4D, the S 2p3/2 and S 2p1/2 peaks both were fitted with two peaks at 161.2/162.1 and 163.3/164.7 eV, respectively. The peaks of 161.2 (S 2p3/2) and 163.3 eV (S 2p1/2) were characteristic of sulfide (Saldanha et al., 2014; Xie et al., 2016), which could be attributed to the S-S bond in CuS (Soares et al., 2017). The peaks at 162.1 (S 2p3/2) and 164.7 eV (S 2p1/2) could be CuS (Kar et al., 2014), and the peak of 168.5 eV could be ascribed to the sulfate species formed by the oxidation of CuS (Zhou et al., 2013).

The UV–vis characterization of PTCA (a), GO (b), Au NPs (c) and PTCA-Au@GO (d) was implemented to prove that PTCA-Au@GO nanomaterials were synthesized successfully. As shown in Fig. S5, PTCA had three ultraviolet absorption peaks in the absorption band of 400–500 nm (curve a), and the ultraviolet absorption peaks were at 466 nm, 438 nm and 412 nm, which accorded with the previous paper (Ma et al., 2017a). Moreover, the three peaks were associated with π-π^* transitions of aromatic group and presented a well-defined vibronic structure (Alessio et al., 2015). GO exhibited a ultraviolet absorption peak at 230 nm (curve b), which was in good agreement with the previous paper (Gao et al., 2013). The characteristic absorption peak was associated with π-π^* transition of the sp^2 carbon (Eda et al., 2010; Lai et al., 2012). The curve c indicated that the maximum absorption peak of the Au NPs was identified at 528 nm. According to curve d, it was observed that the characteristic absorption peaks of PTCA-Au@GO were in good agreement with the peaks of PTCA, GO and Au NPs. Therefore, the results proved that PTCA-Au@GO nanomaterials were synthesized successfully.

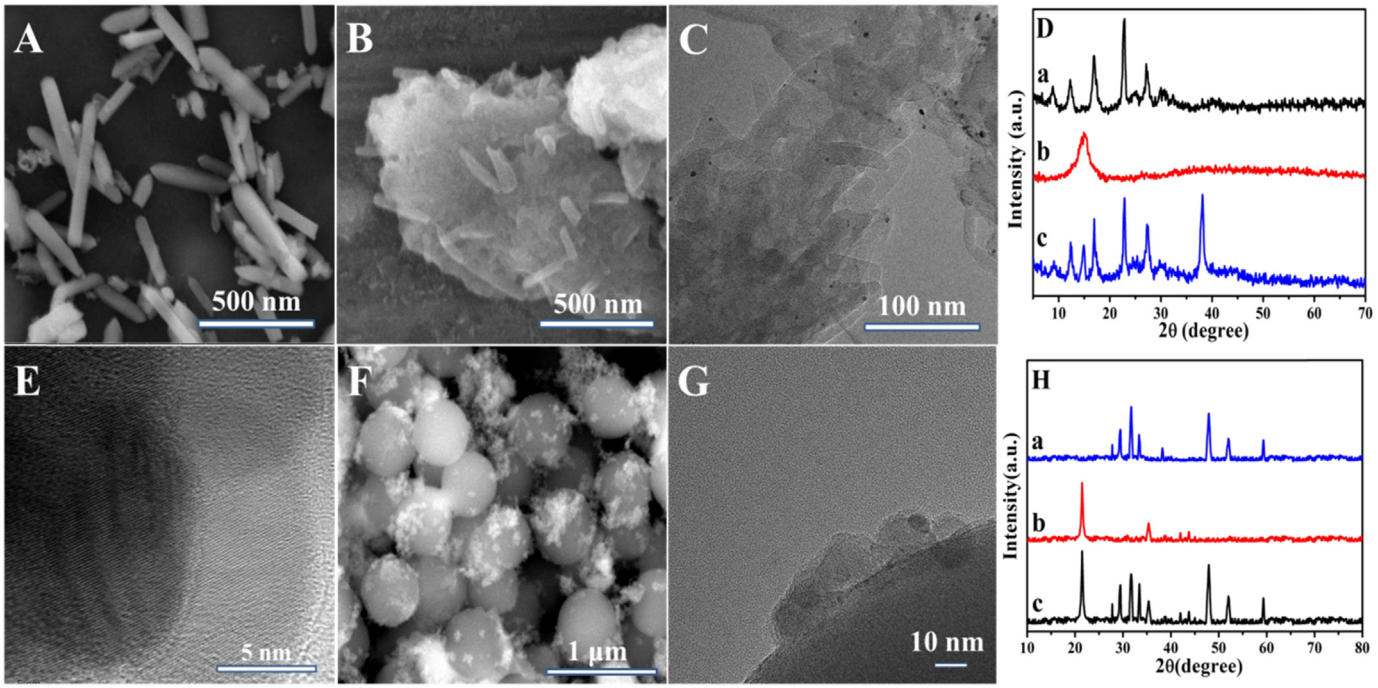

Fig. 2. SEM images of PTCA (A), PTCA@GO (B) and CuS@SiO_2 (F); TEM images of CuS (E), PTCA-Au@GO (C) and CuS-Au@SiO_2 (G); (D) XRD patterns of PTCA (a), GO (b) and PTCA-Au@GO (c); (H) XRD patterns of CuS (a), SiO_2 (b), CuS-Au@SiO_2 (c).

3.2. ECL mechanism of PTCA-Au@GO/$K_2S_2O_8$ system and CuS-Au@SiO_2 enhancing PTCA-Au@GO nanomaterials

As we all know, $K_2S_2O_8$ is a frequently-used cathode coreactant for ECL reactions. When the potential is enough negative, $S_2O_8^{2-}$ is decomposed to generate sulfate radical (SO_4^{2-}) and persulfate anion radical ($SO_4^{\bullet-}$) (Lei et al., 2018). In this work, PTCA acted as cathodic luminescent material to react with the coreactant ($K_2S_2O_8$). The mechanism of PTCA/$S_2O_8^{2-}$ system was as follows: $PTCA^{\bullet-}$ was first generated at the electrode surface, then it reacted with $SO_4^{\bullet-}$ to form the excited state $PTCA^*$ which backed to ground state with emitting light. Nevertheless, PTCA has not strong enough ECL signal in aqueous solution to meet the requirements for trace analysis. Therefore, CuS was used as the co-reaction accelerator which could react with $S_2O_8^{2-}$ to produce more $SO_4^{\bullet-}$, further enhancing the ECL signal of PTCA. As shown in Fig. 3A, PTCA-Au@GO showed better ECL signal than the pure PTCA after GO and Au NPs combined with PTCA. In order to explore the mechanism of CuS in PTCA/$S_2O_8^{2-}$ system, the ECL responses in different solutions were measured. The detailed experimental process was as follows: PTCA solution (a), PTCA + $S_2O_8^{2-}$ solution (b), PTCA + CuS solution (c), PTCA + CuS + $S_2O_8^{2-}$ solution (d), $S_2O_8^{2-}$ solution (e) and CuS + $S_2O_8^{2-}$ solution (f). As shown in Fig. 3B, the electrode was first detected in PTCA solution, and the ECL signal was very low (curve a). Then the ECL intensity has an obvious increase in PTCA + $S_2O_8^{2-}$ solution (curve b), and the reason was that $S_2O_8^{2-}$ was used as the coreactant of PTCA to amplify the ECL signal. Subsequently, the electrode was detected in PTCA + CuS + $S_2O_8^{2-}$ solution (curve d), and the ECL intensity has an obvious increase compared with detecting in PTCA + $S_2O_8^{2-}$ solution. What's more, the ECL signal of PTCA + CuS solution was almost the same with detecting in PTCA solution (curve c), which proved that CuS couldn't react with PTCA directly to affect the ECL signal. Therefore, it was inferred that CuS could enhance the ECL signal by reacting with $S_2O_8^{2-}$. Next, the electrode was detected in $S_2O_8^{2-}$ solution (curve e), and the result was attributed to the emission of singlet oxygen (Dai et al., 2014). Finally, the electrode was detected in CuS + $S_2O_8^{2-}$ solution (curve f), and the ECL intensity was increased compared with that only detected in $S_2O_8^{2-}$ solution. The reason could be that CuS reacted with $S_2O_8^{2-}$ to produce ECL signal. According to these experimental results, it was inferred that CuS could act as co-reaction accelerator to amplify the ECL signal by reacting with $S_2O_8^{2-}$. The possible mechanism of the ECL system contained PTCA, CuS and $K_2S_2O_8$ as the following Eqs. (1)-(5):

$$Cu^{2+} + e^- \rightarrow Cu^+ \quad (1)$$

$$Cu^+ + S_2O_8^{2-} \rightarrow Cu^{2+} + SO_4^{2-} + SO_4^{\bullet-} \text{ (more)} \quad (2)$$

$$PTCA + e^- \rightarrow PTCA^{\bullet-} \quad (3)$$

$$PTCA^{\bullet-} + SO_4^{\bullet-} \rightarrow PTCA^* + SO_4^{2-} \quad (4)$$

$$PTCA^* \rightarrow PTCA + h\nu \quad (5)$$

3.3. ECL and EIS characterization of the immunosensor fabrication

The corresponding ECL-potential curves with different modified electrodes were shown in Fig. 3C, which carried out in PBS (pH = 8.5) containing 0.05 M $K_2S_2O_8$ and 0.1 M KCl. The bare GCE produced a low ECL signal (curve a), and it could be attributed to the system of $S_2O_8^{2-}$/O_2 (Lei et al., 2016; Yao et al., 2009). When GCE was modified with PTCA-Au@GO, the ECL intensity had an obvious increase (curve b). Nevertheless, the ECL intensity was prominently decreased with immobilizing Ab_1, BSA and Aβ on the modified electrode (curve c, curve d and curve e), and the reason was that they both hindered the electron-transfer between coreactant ($K_2S_2O_8$) and luminophor (Wang et al., 2012). Finally, when the modified electrode was incubated with Ab_2-Au@CuS-SiO_2 (curve f), the ECL intensity was increased remarkably. The reason was that CuS could effectively enhance the ECL intensity. The results demonstrated that the ECL immunosensor was fabricated successfully.

Moreover, we could also measure EIS to prove that the ECL immunosensor was fabricated successfully. It was one of the most effective electrochemical methods for identifying the interfacial property of the modified electrode (Ramanavicius et al., 2014). The original curves of EIS with different modified electrodes were shown in Fig. 3D, which carried out in 2.5 mM $[Fe(CN)_6]^{3-/4-}$ and 0.1 M KNO_3. The bare GCE

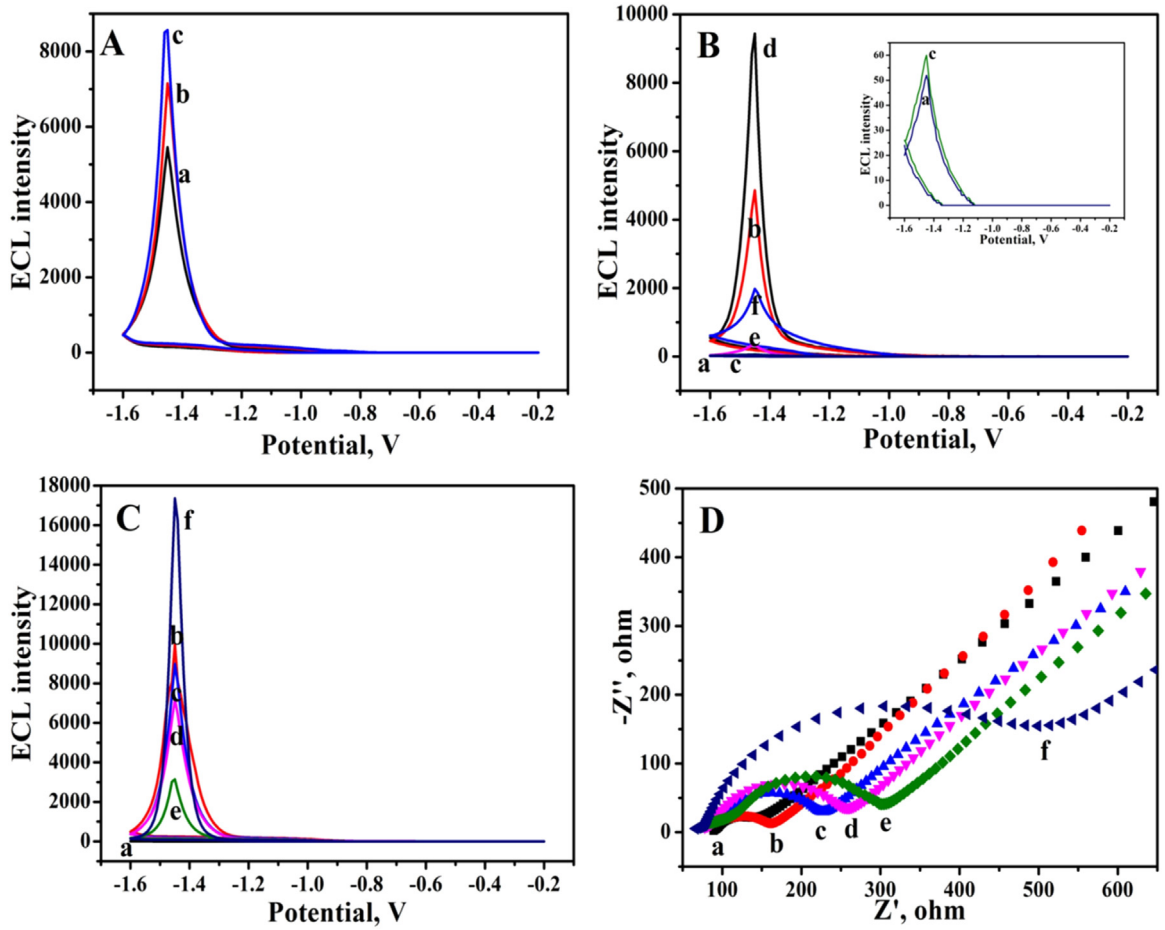

Fig. 3. (A) ECL responses of PTCA (a), PTCA@GO (b) and PTCA-Au@GO (c). (B) ECL responses of GCE measured in PTCA solution (a), PTCA + $S_2O_8^{2-}$ solution (b), PTCA + CuS solution (c), PTCA + CuS + $S_2O_8^{2-}$ solution (d), $S_2O_8^{2-}$ solution (e) and CuS + $S_2O_8^{2-}$ solution (f); (C) ECL responses of bare GCE (a), PTCA-Au@GO/GCE (b), Ab_1/PTCA-Au@GO/GCE (c), BSA/Ab_1/PTCA-Au@GO/GCE (d), Aβ/BSA/Ab_1/PTCA-Au@GO/GCE (e) and Ab_2-Au@CuS-SiO_2/Aβ/BSA/Ab_1/PTCA-Au@GO/GCE (f) in PBS (pH = 8.5) containing 0.1 M KCl and 0.05 M $K_2S_2O_8$; (D) EIS of bare GCE (a), PTCA-Au@GO/GCE (b), Ab_1/PTCA-Au@GO/GCE (c), BSA/Ab_1/PTCA-Au@GO/GCE (d), Aβ/BSA/Ab_1/PTCA-Au@GO/GCE (e) and Ab_2-Au@CuS- SiO_2/Aβ/BSA/Ab_1/PTCA-Au@GO/GCE (f) in 2.5 mM $Fe(CN)_6^{3-/4-}$ and 0.1 M KNO_3.

showed a small semicircle domain (curve a), which was ascribed to the process of free electron transfer. When PTCA-Au@GO was modified on the electrode, the modified electrode exhibited a larger semicircle domain (curve b). The result showed that higher electron transfer resistance of $[Fe(CN)_6]^{3-/4-}$ on PTCA-Au@GO. After Ab_1, BSA, Aβ and Ab_2-Au@CuS-SiO_2 were dropped successively on the modified electrode, the semicircle domains were all increased (curve c, curve d, curve e and curve f). The reason was that the formed protein layer which blocked the electron transfer (Han et al., 2017; Li et al., 2017, 2016; Wang et al., 2017). These results further demonstrated the successful fabrication of the ECL immunosensor.

3.4. Optimization of experimental conditions

To achieve the best experimental results, the experiment conditions should be optimized. First, the effect of pH was investigated from 6.0 to 9.0 to determine the optimal condition. As shown in Fig. 4A, the ECL signal achieved a maximum value at pH 8.5. The reason was that the proton decreased easily at low pH, which caused that the luminescence was inhibited. Moreover, highly pH could affect the activity of the antigens and antibodies, further affected the ECL intensity (Zhang et al., 2017). Therefore, pH 8.5 was selected as the optimal condition for Aβ detection. The concentration of $K_2S_2O_8$ was also an important influencing factor for ECL immunosensor performance. As shown in Fig. 4B, the maximum ECL response appeared at 100 mM. The ECL intensity increased when the concentration of $K_2S_2O_8$ was in the range from 10 mM to 50 mM, and the reason was that more $SO_4^{\bullet-}$ were produced with the increase of $K_2S_2O_8$ concentration, which could produce more excited states PTCA* (Li et al., 2017). Nevertheless, the ECL intensity decreased significantly when the $K_2S_2O_8$ concentration increased to over 50 mM, which was ascribed to that overmuch $S_2O_8^{2-}$ could inhibit the producing of excited state PTCA* (Cheng et al., 2012). Therefore, 50 mM $K_2S_2O_8$ was selected as the optimal condition for Aβ detection. As shown in Fig. 4C, the concentration of PTCA-Au@GO for the fabrication of the immunosensor was investigated. The ECL intensity increased when the concentration of PTCA-Au@GO increased from 0.5 mg/mL to 1 mg/mL, then decreased with a further increase of PTCA-Au@GO concentration, which attributed to the self-absorption effect of the luminophor (Hua et al., 2009). Moreover, excessive PTCA-Au@GO could hinder the electron transfer. Consequently, 1 mg/mL PTCA-Au@GO was selected as the optimal condition for the fabrication of the immunosensor. Finally, the concentration of CuS-Au@SiO_2 was investigated for the fabrication of the immunosensor. The ECL intensity changed with the concentrations of CuS-Au@SiO_2 when the concentrations of PTCA was equal. As shown in Fig. 4D, the ECL signal difference increased gradually when the concentration of CuS-Au@SiO_2 changed from 0.5 mg/mL to 2.0 mg/mL, then decreased with further increase of CuS-Au@SiO_2 concentration, and the ECL intensity difference reached the maximum at 2.0 mg/mL. The reason was that interface electron transfer resistance increased along with the increase of the concentration of CuS-Au@SiO_2, but the electrical conductivity decreased as a result of excessive CuS-Au@SiO_2 (Zhang et al., 2014).

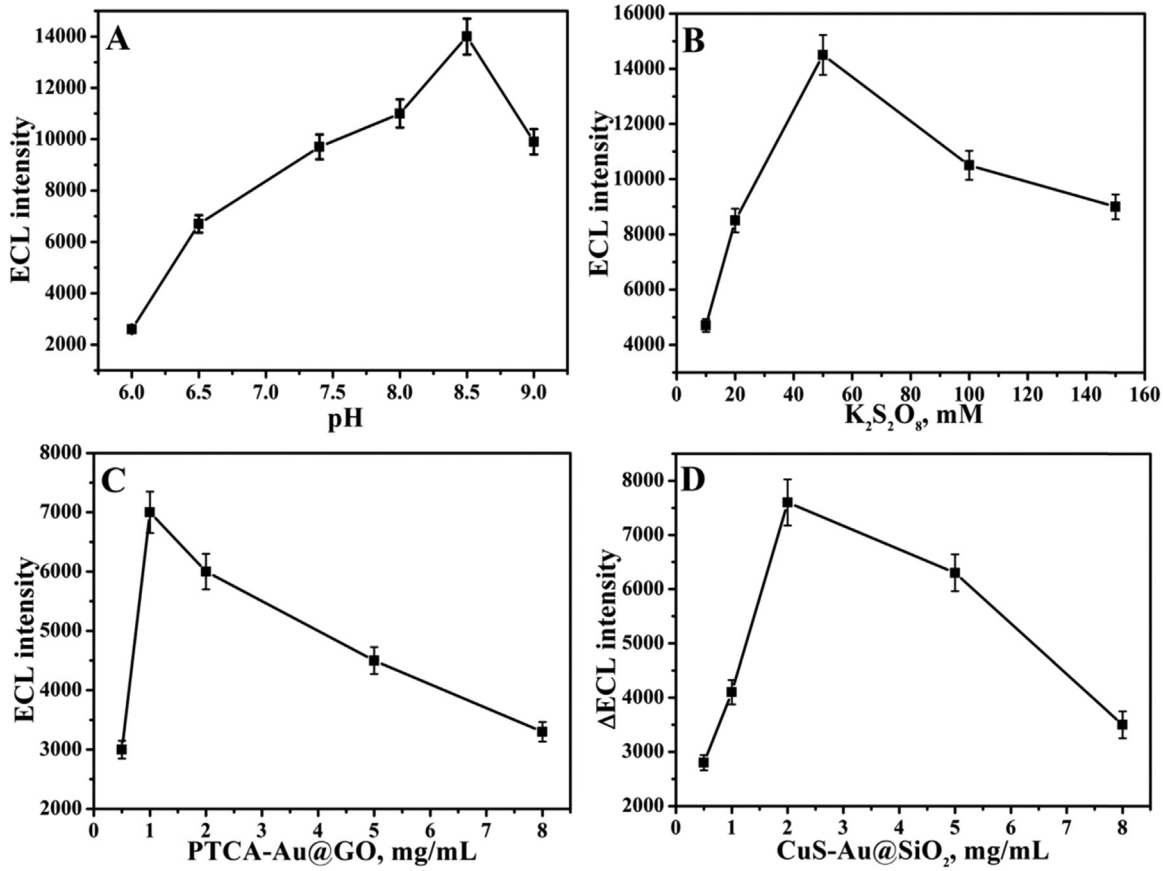

Fig. 4. The effect of pH (A), $K_2S_2O_8$ (B) and PTCA-Au@GO (C) on the responses of ECL intensity from PTCA-Au@GO/GCE; (D) The effect of CuS-Au@SiO_2 on the signal of ECL immunosensor. (ΔECL intensity was the difference between PTCA-Au@GO/GCE and Ab_2-Au@CuS-SiO_2/Aβ/BSA/Ab_1/PTCA-Au@GO/GCE). Error bars = RSD (n = 3).

Therefore, 2.0 mg/mL CuS-Au@SiO_2 was selected as the optimal condition for Aβ detection.

3.5. Performance of the immunosensor

In this work, the analytical performance of the proposed immunosensor was investigated by incubating different concentrations of Aβ under the optimization conditions. As shown in Fig. 5A, the ECL intensity increased gradually with the increasing concentrations of Aβ from 50 fg/mL to 25 ng/mL (curve a-k). Moreover, the ECL intensity was correlated with the exponential value of Aβ concentrations, and the linear response range was from 50 fg/mL to 25 ng/mL. As shown in Fig. 5B, the linear equation was I = 2145.02 lnc + 11795.42, with a correlation coefficient of 0.9961 and a detection limit of 18 fg/mL (S/N = 3). As shown in Table S1, it was observed that the proposed immunosensor showed better detection linear range and detection limit compared with previous works. This indicated that the strategy exhibited high sensitivity and great potential for the precise detection of Aβ.

3.6. Stability, selectivity and reproducibility

Operational stability is one of the most main portion for the fabrication of the immunosensor (Wu et al., 2018). As shown in Fig. 5C, the stability of the ECL immunosensor was investigated by detecting 5 ng/mL Aβ under 11 cycles of successive potential scans. It was calculated that the relative standard deviation of ECL intensity was 1.06%, which indicated that the sensing signal was quite reliable.

To investigate the selectivity of the developed immunosensor, carcinoembryonic antigen (CEA), alpha fetoprotein (AFP), bovine serum albumin (BSA), glucose (Glu), Immunoglobulin G (IgG) and human serum albumin (HSA) were used as the interferences. As shown in Fig. 5D, the ECL signal of the target Aβ (1 ng/mL) was much higher than that of CEA (1 ng/mL), AFP (1 ng/mL), BSA (1 ng/mL), Glu (1 ng/mL), IgG (1 ng/mL) and HSA (1 ng/mL). Furthermore, the ECL intensity with a mixture solution (1 ng/mL Aβ containing 100 ng/mL CEA, 100 ng/mL AFP, 100 ng/mL BSA, 100 ng/mL Glu, 100 ng/mL IgG and 100 ng/mL HSA) were almost the same with that incubating with Aβ. Therefore, the selectivity of the developed immunosensor was excellent.

As shown in Fig. S6, the repeatability of the ECL immunosensor was investigated by seven prepared electrodes for the detection of Aβ (0.01 ng/mL). The results indicated that the RSD of measurements was less than 5%, which proved that the repeatability of the immunosensor was excellent.

3.7. Analysis of clinical serum samples

To investigate the real sample analysis of the fabricated immunosensor, the standard addition method was conducted for the detection of Aβ in human serum. Prior to measurement, the samples were centrifugated by loading into a centrifugal filtration tube to obtain the supernatant. Subsequently, the content of Aβ in the samples was detected by the proposed immunosensor according to the relation between the current and the concentration. As described in Table S2, the recoveries were ranging from 99.6% to 101% and the RSD was in the range of 1.01–1.51%, which indicated that the developed immunosensor was feasible for the detection of Aβ in human serum samples.

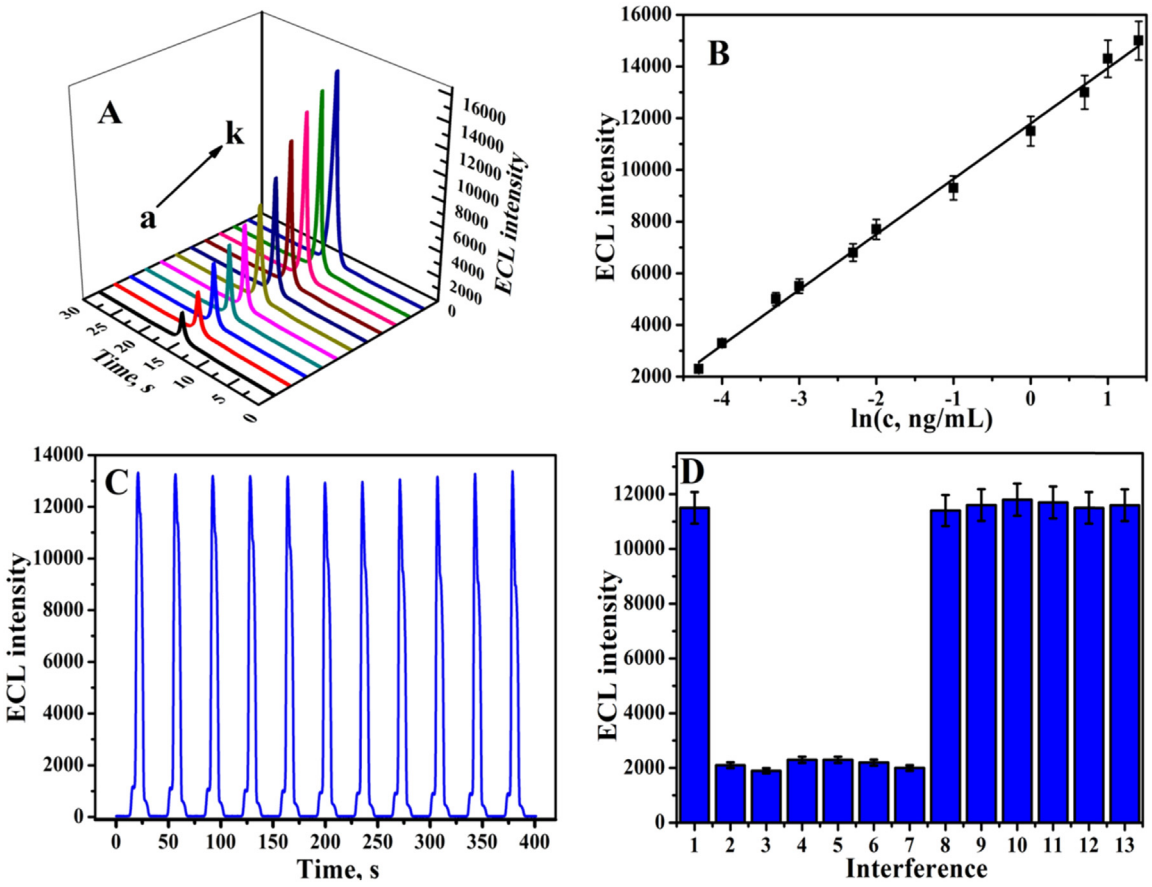

Fig. 5. (A) ECL responses of the immunosensor in different concentrations of Aβ, from a to k: 0.00005, 0.0001, 0.0005, 0.001, 0.005, 0.01, 0.1, 1, 5, 10 and 25 ng/mL; (B) Calibration curve of the immunosensor for different concentrations of Aβ; (C) Stability of ECL emissions under continuous scanning for 11 cycles in PBS (pH = 8.5) containing 0.1 M KCl and 0.05 M $K_2S_2O_8$ for the detection of 5 ng/mL Aβ; (D) The ECL intensity responses of the immunosensor to 1 ng/mL Aβ (1), 1 ng/mL CEA (2), 1 ng/mL AFP (3), 1 ng/mL BSA (4), 1 ng/mL Glu (5), 1 ng/mL IgG (6), 1 ng/mL HSA (7), 1 ng/mL Aβ + 100 ng/mL CEA(8), 1 ng/mL Aβ + 100 ng/mL AFP (9), 1 ng/mL Aβ + 100 ng/mL BSA (10), 1 ng/mL Aβ + 100 ng/mL Glu (11), 1 ng/mL Aβ + 100 ng/mL IgG (12) and 1 ng/mL Aβ + 100 ng/mL HSA (13). Error bars = RSD (n = 3).

4. Conclusion

In conclusion, a novel and efficient enhancing ECL immunosensor for sensitively detecting Aβ was successfully developed. CuS was used as a novel co-reaction accelerator in PTCA-$K_2S_2O_8$ system which can react with the coreactant ($S_2O_8^{2-}$) to produce more $SO_4^{\cdot-}$, further enhancing the ECL signal. Besides, Au@GO exhibited large specific surface area and excellent electrical conductivity which can load large amounts of PTCA and antibodies to improve the ECL efficiency. The proposed immunosensor showed better detection linear range and detection limit compared with previous works, which indicated that the strategy exhibited high sensitivity and great potential for the precise detection of Aβ. Moreover, the fabricated immunosensor exhibited excellent stability, selectivity and acceptable reproducibility, which suggested its potential applications in real samples.

Acknowledgements

This work was supported by the National Key Scientific Instrument and Equipment Development Project of China (No. 21627809), and the National Natural Science Foundation of China (No. 21675063; 21575050).

Appendix A. Supplementary material

Supplementary data associated with this article can be found in the online version at doi:10.1016/j.bios.2018.10.068.

References

Alessio, P., Braunger, M.L., Aroca, R.F., Olivati, C.D.A., Constantino, C.J.L., 2015. J. Phys. Chem. C 119 (21) (12055-12046).
Cai, Z., Xu, W., Li, F., Yao, Q., Chen, X., 2016. ACS Sustain. Chem. Eng. 5 (1), 571–579.
Cheng, C., Huang, Y., Tian, X., Zheng, B., Li, Y., Yuan, H., Xiao, D., Xie, S., Choi, M.M., 2012. Anal. Chem. 84 (11), 4754–4759.
Chung, S.H., Lee, D.W., Kim, M.S., Lee, K.Y., 2011. J. Colloid Interface Sci. 355 (1), 70–75.
Cowie, M.R., Jourdain, P., Maisel, A., Dahlstrom, U., Follath, F., Isnard, R., Luchner, A., Mcdonagh, T., Mair, J., Nieminen, M., 2003. Eur. Heart J 24 (19), 1710–1718.
Dai, H., Xu, G., Zhang, S., Gong, L., Li, X., Yang, C., Lin, Y., Chen, J., Chen, G., 2014. Biosens. Bioelectron. 61 (20), 575–578.
Dubale, A.A., Tamirat, A.G., Chen, H.M., Berhe, T.A., Pan, C.J., Su, W.N., Hwang, B.J., 2016. J. Mater. Chem. A 4 (6), 2205–2216.
Dutta, A.K., Das, S., Samanta, S., Samanta, P.K., Adhikary, B., Biswas, P., 2013. Talanta 107 (2), 361–367.
Eda, G., Lin, Y.Y., Mattevi, C., Yamaguchi, H., Chen, H.A., Chen, I.S., Chen, C.W., Chhowalla, M., 2010. Adv. Mater. 22 (4), 505–509.
Feng, C., Le, Z., Yang, M., Song, X., Hui, Z., Zhe, J., Sun, K., Gao, L., 2015. ACS Appl. Mater. Interfaces 7 (29), 15726–15734.
Gao, N., Chen, Y., Jiang, J., 2013. ACS Appl. Mater. Interfaces 5 (21), 11307–11314.
Goel, S., Chen, F., Cai, W., 2013. Small 10 (4), 631–645.
Han, Q., Wang, R., Xing, B., Zhang, T., Khan, M.S., Wu, D., Wei, Q., 2017. Biosens. Bioelectron. 99, 493–499.
Hong, Y., Zhang, J., Huang, F., Zhang, J., Wang, X., Wu, Z., Lin, Z., Yu, J., 2015. J. Mater. Chem. A 3 (26), 13913–13919.
Hua, L., Han, H., Chen, H., 2009. Electrochim. Acta 54 (5), 1389–1394.
Jana, A., Devi, K.S.P., Maiti, T.K., Singh, N.D.P., 2012. J. Am. Chem. Soc. 134 (18), 7656–7659.
Jana, A., Nguyen, K.T., Li, X., Zhu, P., Tan, N.S., Ågren, H., Zhao, Y., 2014. ACS Nano 8 (6), 5939–5952.
Jang, H.R., Wark, A.W., Baek, S.H., Chung, B.H., Lee, H.J., 2014. Anal. Chem. 86 (1), 814–819.

Jia, C., Qiao, C., Gao, C., Zhang, M., Bo, Q., Qiu, H., 2015. J. Mater. Chem. B 3 (6), 964–967.
Kar, P., Farsinezhad, S., Zhang, X., Shankar, K., 2014. Nanoscale 6 (23), 14305–14318.
Karpenko, A., Leppelt, R., Cai, J., Plzak, V., Chuvilin, A., Kaiser, U., Behm, R.J., 2007. J. Catal. 250 (1), 139–150.
Lai, Q., Zhu, S., Luo, X., Zou, M., Huang, S., 2012. AIP Adv. 2 (3), 023146.
Lee, H., Sang, W.Y., And, E.J.K., Park, J., 2007. Nano Lett. 7 (3), 778–784.
Lei, Y.M., Wen, R.X., Zhou, J., Chai, Y.Q., Yuan, R., Zhuo, Y., 2018. Anal. Chem. 90 (11), 6851–6858.
Lei, Y.M., Zhao, M., Wang, A., Yu, Y.Q., Chai, Y.Q., Yuan, R., Zhuo, Y., 2016. Chem. - Eur. J. 22 (24), 8207–8214.
Li, F., Yang, H., Shan, C., Zhang, Q., Han, D., Ivaska, A., Li, N., 2009. J. Mater. Chem. 19 (23), 4022–4025.
Li, X., Lu, P., Wu, B., Wang, Y., Wang, H., Du, B., Pang, X., Wei, Q., 2018. Biosens. Bioelectron. 40–47.
Li, X., Wang, Y., Shi, L., Ma, H., Zhang, Y., Du, B., Wu, D., Wei, Q., 2017. Biosens. Bioelectron. 96, 113–120.
Li, X., Yu, S., Yan, T., Zhang, Y., Du, B., Wu, D., Wei, Q., 2016. Biosens. Bioelectron. 89, 1020–1025.
Liu, X., Cui, S., Sun, Z., Ren, Y., Zhang, X., Du, P., 2016. J. Phys. Chem. C 120 (2), 831–840.
Ma, H., Chen, Y., Wang, H., Wang, X., Zhang, X., Han, X.X., He, C., Zhao, B., 2017a. J. Phys. Chem. C 121 (46), 25788–25794.
Ma, M., Ge, R., Ji, X., Ren, X., Liu, Z., Asiri, A.M., Sun, X., 2017b. ACS Sustain. Chem. Eng. 5 (11), 9625–9629.
Marcano, D.C., Kosynkin, D.V., Berlin, J.M., Sinitskii, A., Sun, Z., Slesarev, A., Alemany, L.B., Lu, W., Tour, J.M., 2010. ACS Nano 4 (8), 4806–4814.
Mazin, I.I., 2012. Phys. Rev. B 85 (11), 117–122.
Nhan, H.S., Chiang, K., Koo, E.H., 2015. Acta Neuropathol. 129 (1), 1–19.
Nie, G., Li, Z., Lu, X., Lei, J., Zhang, C., Wang, C., 2013. Appl. Surf. Sci. 284 (11), 595–600.
Nishikimi, T., Okamoto, H., Nakamura, M., Ogawa, N., Horii, K., Nagata, K., Nakagawa, Y., Kinoshita, H., Yamada, C., Nakao, K., 2013. PLoS One 8 (1), e53233.
Qiao, L., Jin, J., Zhang, J., 2013. ACS Appl. Mater. Interfaces 5 (11), 5002–5008.
Ramanavicius, A., Genys, P., Ramanaviciene, A., 2014. Electrochim. Acta 146, 659–665.
Saldanha, P.L., Brescia, R., Prato, M., Li, H., Povia, M., Manna, L., Lesnyak, V., 2014. Chem. Mater. 26 (3), 1442–1449.
Selkoe, D.J., 2001. Physiol. Rev. 81 (2), 741–766.
Selkoe, D.J., Schenk, D., 2003. Annu. Rev. Pharmacol. Toxicol. 43 (1), 545–584.
Shuang, W., Wang, X., Wang, G., Guo, Y., Wang, K., Yang, G., Zhu, L., Yang, L., 2015. J. Mater. Chem. B 3 (27), 5603–5607.
Soares Jr,, A.L., Dos Santos, E.C., Moralesgarcía, A., Heine, T., De Abreu, H.A., Duarte, H.A., 2017. 2D Mater. 4 (1), 015041.
Tan, G., Wang, K., 2010. Curr. Nanosci. 6 (2), 163–168.
Thuy, U.T.D., Liem, N.Q., Parlett, C.M.A., Lalev, G.M., Wilson, K., 2014. Catal. Commun. 44 (1), 62–67.
Tian, H., Zhang, X., Scott, J., Ng, C., Amal, R., 2014. J. Mater. Chem. A 2 (18), 6432–6438.
Wang, H., Yuan, R., Chai, Y., Niu, H., Cao, Y., Liu, H., 2012. Biosens. Bioelectron. 37 (1), 6–10.
Wang, X., Xu, R., Sun, X., Wang, Y., Ren, X., Du, B., Wu, D., Wei, Q., 2017. Biosens. Bioelectron. 96, 239–245.
Wang, Y., Yan, T., Gao, L., Cui, L., Hu, L., Yan, L., Du, B., Wei, Q., 2016. Desalin. Water Treat. 57 (9), 3975–3984.
Wu, D., Wei, Y., Ren, X., Ji, X., Liu, Y., Guo, X., Liu, Z., Asiri, A.M., Wei, Q., Sun, X., 2018. Adv. Mater. 30 (9), 1705366.
Xie, Y., Riedinger, A., Prato, M., Casu, A., Genovese, A., Guardia, P., Sottini, S., Sangregorio, C., Miszta, K., Ghosh, S., 2016. J. Am. Chem. Soc. 135 (46), 17630–17637.
Yao, W., Wang, L., Wang, H., Zhang, X., 2009. Electrochim. Acta 54 (2), 733–737.
Zhang, H., Zuo, F., Tan, X., Xu, S., Yuan, R., Chen, S., 2017. Biosens. Bioelectron. 104, 65–71.
Zhang, S., Ma, H., Yan, L., Cao, W., Yan, T., Wei, Q., Du, B., 2014. Biosens. Bioelectron. 59 (9), 335–341.
Zhao, K., Liu, S., Ye, G., Gan, Q., Zhou, Z., He, Z., 2017. J. Mater. Chem. A 6 (5), 2166–2175.
Zhou, G., Yin, L.C., Wang, D.W., Li, L., Pei, S., Gentle, I.R., Li, F., Cheng, H.M., 2013. ACS Nano 7 (6), 5367–5375.
Zhou, L.L., Fang, T., Cao, J.P., Zhu, Z.H., Su, X.T., Zhan, S.Z., 2015. J. Power Sources 273 (273), 298–304.
Zhuo, Y., Liao, N., Chai, Y.Q., Gui, G.F., Zhao, M., Han, J., Xiang, Y., Yuan, R., Chem, A., 2014. Anal. Chem. 86 (2), 1053–1060.